Performance Enhancement of a Battery-Grid Connected SiC MMC for DC Microgrid Systems

Wang, Yang; Aksoz, Ahmet; Geury, Thomas; El Baghdadi, Mohamed; Hegazy, Omar

Published in:
2021 Sixteenth International Conference on Ecological Vehicles and Renewable Energies (EVER)

DOI:
10.1109/EVER52347.2021.9456612

Publication date:
2021

2021 Sixteenth International Conference on Ecological Vehicles and Renewable Energies (EVER)

Performance Enhancement of a Battery-Grid Connected SiC MMC for DC Microgrid Systems

Yang Wang[1,2], Ahmet Aksoz[1,2], Thomas Geury[1,2], Mohamed El Baghdadi[1,2], Omar Hegazy[1,2]
[1]ETEC Department & MOBI Research Center, Vrije Universiteit Brussel (VUB), Pleinlaan 2,1050 Brussels, Belgium.
[2]Flanders Make, 3001 Heverlee, Belgium
Email: Omar.Hegazy@vub.be

***Abstract*—The modular multilevel converter (MMC) is a recently developed and advanced alternative power converter in the high and medium voltage applications. It is suitable for the DC microgrid systems to effectively integrate the distributed power systems such as battery energy storage systems, wind power systems，and solar photovoltaic systems. In this paper, a battery-based SiC-MMC with 17 submodules per arm for efficient DC-microgrid systems is investigated in terms of its mathematical modelling, control and thermal modeling. The modeling and analysis of the MMC show that the output voltage and output current have good performance with low harmonic distortion. The comparison of power losses shows that the SiC semiconductors have superior performance over conventional Si-based switches in the high-power applications.**

Keywords*— *Modular multilevel converter (MMC); SiC MMC; modeling and control; power losses; DC microgrid systems.

I. INTRODUCTION

The Modular Multilevel Converters (MMCs), thanks to their promising characteristics of quality output performance, reduced voltage and current rating demand for the semiconductors, together with modular and scalable design, have gained increasing research interest since the first MMC proposal published by Lesnicar and Marquardt in 2002 [1]. The MMCs have been introduced progressively in the applications with medium and high-voltage and power ratings, for instance, high-voltage direct current (HVDC) networks [2], static synchronous compensators (STATCOM) [3], smart grids [4], wind turbine farms [5], solar photovoltaic plants [6], and battery energy storage systems (BESS) [7]. The DC microgrid systems are local scaled-down direct current power supply systems with advantages of independent operating capability, improved reliability, lower electricity cost and lower carbon emissions [8]. The MMCs are expected to be attractive power interfaces with flexible and scalable design in terms of voltage and current for the DC microgrids. Some recent literatures proposed the MMC with integrated BESS which boosts the distribution DC/AC microgrid and facilitates the microgrid stability. The researchers in [7] first investigated the MMC with distributed battery sources and compared it with the cascaded converter and the MMC with centralized BESS, and emphasized that the MMC with distributed BESS yields the highest efficiency, reliability and versatility. [9] presents a battery-grid MMC protype with a rated apparent output power of 2 kVA and experimental results for verification. The research group of Feng Gao explored the control of battery-based MMC and provided methods to balance the battery state of charge and health (SoC & SoH) [10]–[13].

Meanwhile, Silicon Carbide (SiC) and Gallium Nitride (GaN) based Wide Bandgap (WBG) switches have superior advantages in electrical and thermal conductivities, which enable them operating under the high-voltage, high-frequency and high-temperature conditions when compared to conventional silicon-based switches [14]. Nowadays, the SiC switches are replacing the Si-based devices in the high-power and medium-frequency applications, and the GaN modules are occupying the market in the low-power and high-frequency applications. Resullt

This paper firstly presents the configuration and operation of the battery-based SiC MMC connected to the DC microgrid (Section 2) and investigates the system mathematical modeling and control together with the calculation of power losses (Section 3). Section 4 provides the simulation results concerning output voltage and current, and analyzes the thermal performance by comparing the power losses of the SiC and Si-based semiconductors.

II. MMC CONFIGURATION AND OPERATION

The configuration of the SiC MMC for a DC microgrid provided by the battery DC sources is shown in Fig. 1a, which includes three phase-legs and an AC output terminal. Each leg/phase of the SiC MMC has 2 symmetric arms series-connected in the upper and lower branches. The two symmetric branches are composed of a series of identical submodules (SMs) along with an arm inductor to restrain the high-frequency current components. The SM is the fundamental element of an

978-1-6654-4902-1/21/©2021 European Union

MMC, and a wide variety of submodule topologies have been proposed in the literature reviews serving as half-bridge SM (HBSM), full-bridge SM (FBSM), self-balancing SM (SBSM), double-clamp SM (DCSM), and etc. Among these SM configurations, the HBSM is the most used module in the interest of system simplification and cost reduction [15]. The HBSM consists of two semiconductors with two freewheel diodes and a battery pack. Fig. 1b shows the conventional Si-based SM configuration and Fig. 1c is the proposed SiC-based MMC SM configuration.

The HBSM is also referred to as the chopper cell and its module voltage can be shifted to the battery voltage or zero , depending on whether the battery is inserted or bypassed. The operating states of the half bridge configuration are summarized in Table 1.

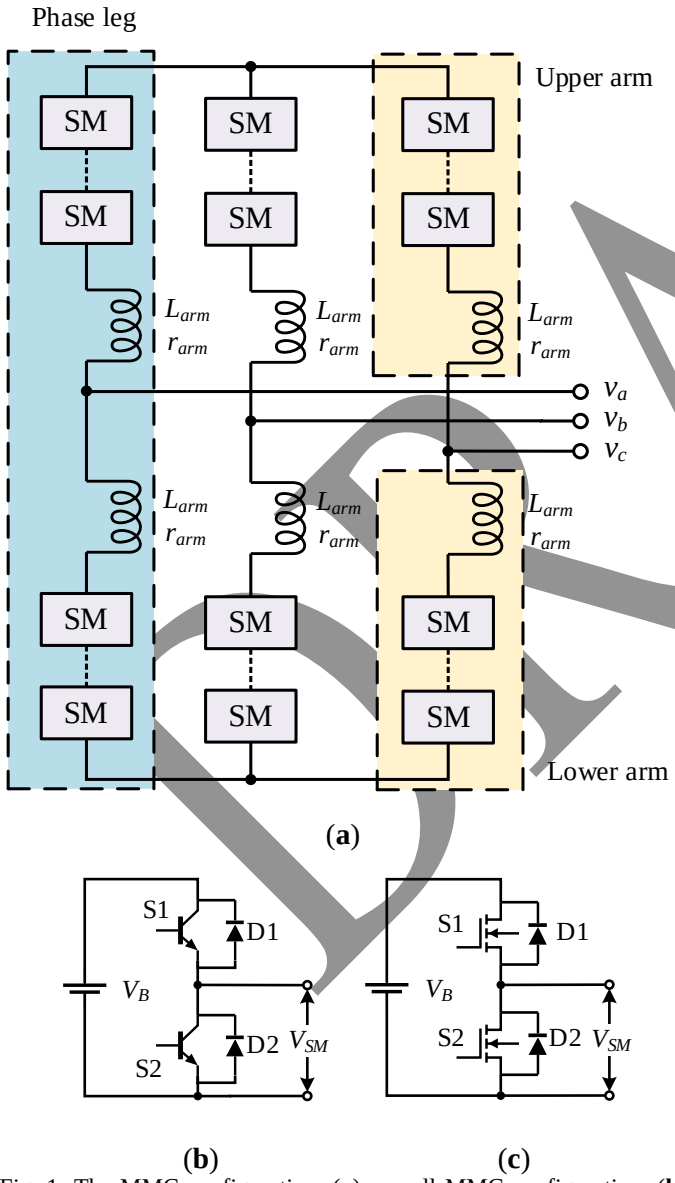

Fig. 1: The MMC configuration: (**a**) overall MMC configuration; (**b**) the conventional Si-based SM configuration; (**c**) the selected SiC-based SM configuration.

TABLE 1: OPERATING STATES OF THE HBSM

HBSM state	S1 state	S2 state	i_{SM} state	i_B state	V_B state	V_{SM} state
Inserted	On	Off	>0	>0	$V_B \uparrow$	V_B
Inserted	On	Off	<0	<0	$V_B \downarrow$	V_B
Bypassed	Off	On	>0	0	$V_B \approx$	0
Bypassed	Off	On	<0	0	$V_B \approx$	0

III. MODELING AND CONTROL

The output and circulating currents can be obtained by the upper and lower arm currents as

$$i_x = i_{xu} - i_{xl} \tag{1}$$

$$i_{cirx} = \frac{i_{xu} + i_{xl}}{2} \tag{2}$$

where i_x ($x = \{a, b, c\}$) are the output currents, i_{xu} and i_{xl} stand for the currents of the upper and lower branches, and i_{cirx} represent the circulating currents.

Based on Kirchoff's voltage law, the voltages v_{xu} and v_{xl} of the upper and lower branches can be determined by

$$v_{xu} = NV_B - v_x - L_{arm}\frac{di_{xu}}{dt} - r_{arm}i_{xu} \tag{3}$$

$$v_{xl} = NV_B + v_x - L_{arm}\frac{di_{xu}}{dt} - r_{arm}i_{xu} \tag{4}$$

where v_x is the output voltage, V_B represents the submodule battery voltage, N donates the number of SMs in each arm branch, and L_{arm} and r_{arm} are the inductance and resistance in each arm, respectively.

The MMC output three-phase terminal is connected to the grid AC source. The MMC active and reactive power can be regulated by using current control on the basis of instantaneous power theory coordinated in the synchronous rotating dq-frame. The relationship between active/reactive power and decoupled dq current can be expressed as

$$P = \frac{3}{2}v_{sd}i_d \tag{5}$$

$$Q = -\frac{3}{2}v_{sq}i_q \tag{6}$$

where v_{sd} and v_{sq} are the decoupled grid voltage in dq axes, similarly, i_d and i_q donate the decoupled dq-frame current.

The voltages expressed in the dq coordinate system can be noted as

$$v_d = v_{sd} + L_s \frac{di_d}{dt} + r_s i_d - \omega L_s i_q \quad (7)$$

$$v_q = v_{sq} + L_s \frac{di_q}{dt} + r_s i_q + \omega L_s i_d \quad (8)$$

where v_d and v_q donate the decoupled dq-frame voltage, ω represnets the grid angular frequency, and L_S and r_S are the grid side inductance and resistance. The block diagram of the power control for the grid tied MMC is shown in Fig. 2.

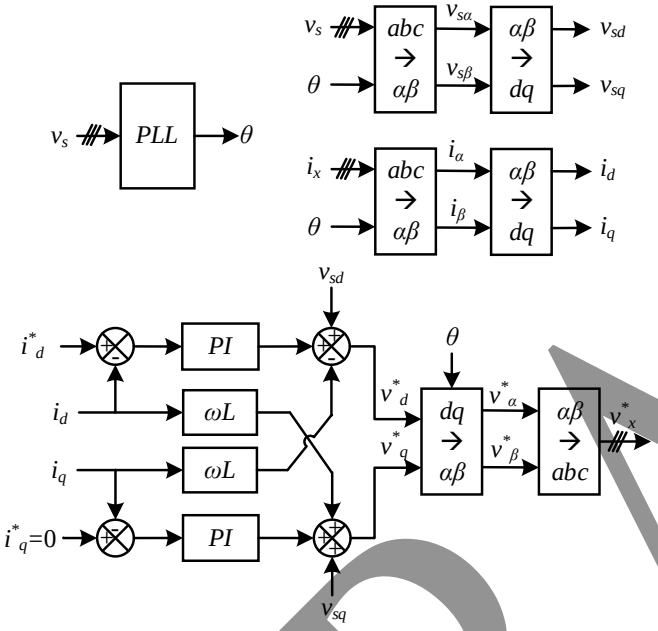

Fig. 2: Block diagram of power control for the grid tied MMC.

The generated voltage reference is processed in the modulator to produce gate signals for each submodule of the MMC. The modulation scheme employed in this paper is PSC-PWM in which N identical triangular carriers are utilized and arranged with a phase shifting $2\pi/N$ in horizon. Through the comparison between the reference signals with the carrier waveforms, the converter can create (N+1)-level output voltage or (2N+1)-level output voltage, which are different with respect to the arranged interval angle π/N of the carrier signals in the upper and lower branches [12]. Fig. 3a shows an example of the PSC-PWM when there are 8 submodules in the upper or lower branch and so 8 carrier signals in one fundamental frequency period. Fig. 3b illustrates the generated PWM waveform in the arm branch after the comparison between the reference signals with the carrier signals.

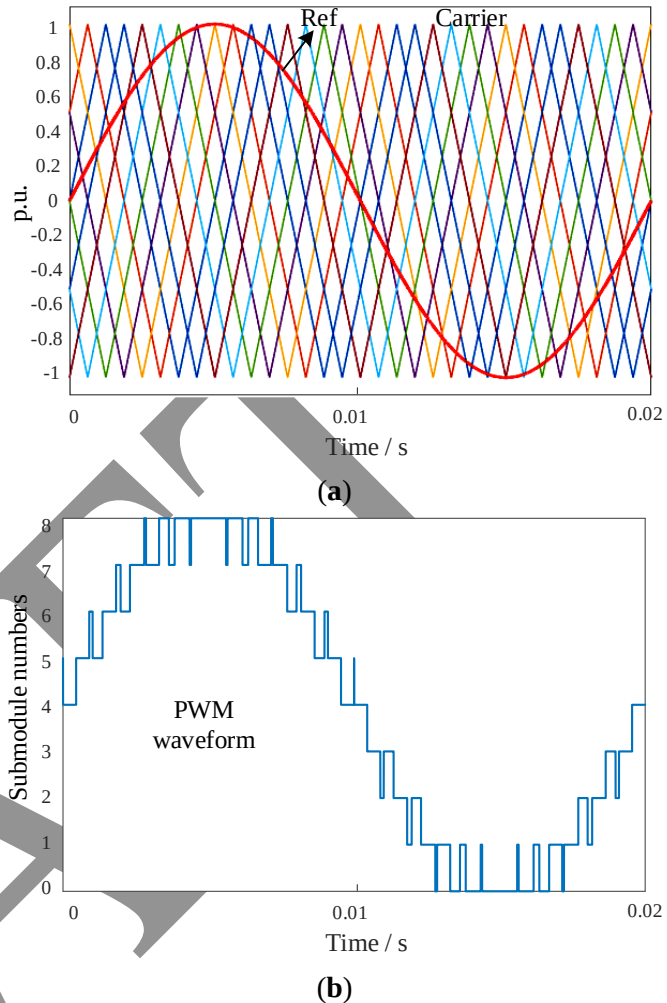

Fig. 3: Illustration of the PSC-PWM: (**a**) the PSC-PWM reference signal and carrier signals; (**b**) the generated PWM waveform.

IV. Power Losses

Thermal management has great importance for the high-power density applications with respect to the performance of power devices, energy efficiency and cost. A power losses calculation model of switching modules can contribute to an accurate model of the electrical and thermal behavior of the power modules. The total power losses of transistors contain the conduction losses and the switching losses [15]. The conduction losses can be yielded as the product of semiconductor voltage and semiconductor instantaneous current in each fundamental frequency period T.

$$P_{conT} = \frac{1}{T}\int_{t_0}^{t_0+T} i_T(t) v_T(t) dt = \frac{1}{T}\int_{t_0}^{t_0+T} i_T(t)(V_{T0} + R_T i_T(t)) dt \quad (9)$$

$$P_{conD} = \frac{1}{T}\int_{t_0}^{t_0+T} i_F(t)v_F(t)dt = \frac{1}{T}\int_{t_0}^{t_0+T} i_F(t)(V_{D0} + R_D i_F(t))dt \quad (10)$$

where P_{conT} and P_{conD} donate the conduction loss of the switch and its freewheeling diode, respectively, i_T and i_F represent the conduction current, V_{T0} and V_{D0} are the saturation voltage, and R_T and R_D donate the slope resistance.

The switching energies in each switch-on and switch-off transition contributes to the switching losses of the device switch part and the reverse recovery energy contributes to that of the diode part. The switching energies and reverse recovery energy of each single switching event are related to the device voltage, current and temperature provided by the manufacturer datasheet. For the sake of model simpification and fast calculation, the influence of temperature on the power losses is not taken into consideration. Thus, the calculation switching loss of the switch and diode parts involves energy loss per switching event and the counts of switching transitions, which is expressed as

$$P_{onT} = \frac{1}{T}\sum_{i=1}^{N_i}\left\{\frac{v_T(t)}{v_{T\_ref}}E_{on}(i_T(t))\right\} = \frac{1}{T}\sum_{i=1}^{N_i}\left\{\frac{v_T(t)}{v_{T\_ref}}\frac{i_T(t)}{i_{T\_ref}}E_{on}(i_{T\_ref})\right\} \quad (11)$$

$$P_{offT} = \frac{1}{T}\sum_{i=1}^{N_i}\left\{\frac{v_T(t)}{v_{T\_ref}}E_{off}(i_T(t))\right\} = \frac{1}{T}\sum_{i=1}^{N_i}\left\{\frac{v_T(t)}{v_{T\_ref}}\frac{i_T(t)}{i_{T\_ref}}E_{off}(i_{T\_ref})\right\} \quad (12)$$

$$P_{recD} = \frac{1}{T}\sum_{i=1}^{N_i}\left\{\frac{v_D(t)}{v_{D\_ref}}E_{rec}(i_D(t))\right\} = \frac{1}{T}\sum_{i=1}^{N_i}\left\{\frac{v_D(t)}{v_{D\_ref}}\frac{i_F(t)}{i_{F\_ref}}E_{off}(i_{F\_ref})\right\} \quad (13)$$

where P_{onT} and P_{offT} are the switch-on and switch-off losses of the switch, P_{recD} is the switching losses of the diode, E_{on} and E_{off} donate the switch-on and switch-off energy losses per switching transition, and E_{rec} is the reverse recovery energy of the diode. The calculation model employs look-up table technique to approximate the energy losses values based on the reference voltage and current.

V. Simulation Results

In order to verify the SiC MMC performance and calculate the power losses of the SiC switches in the MMC, the SiC MMC is modelled and simulated in Matlab/Simulink®. In addition, the main simulation parameters are listed in Table 2.

TABLE 2: SIMULATION PARAMETERS

Parameters	Values
No. of submodules per arm	17
Battery voltage (MMC module)	832 V
Nominal power	6.36 MW
Grid line-to-line voltage	10 kV (RMS)
Line frequency	50 Hz
Arm inductance	2 mH
Modulation method	PSC-PWM
Switching frequency	10 kHz

The grid side AC voltage is 10 kV RMS [16] (14.14 kVp-p) and the variable power based grid side AC current results together with the total harmonic distortion (THD) are demonstrated in Fig. 4. Fig. 4a illustrates that the AC terminal of the SiC MMC outputs three-phase 35-level voltages providing low harmonic distortion (THD is 3.11% shown in Fig. 4c) on the grid voltage. In addition, the three-phase AC currents, which also present low harmonic distortion, give appropriate responses to the reference current inputs, as displayed in Fig. 4 b. Fig. 4d gives an example of THD when the output current is aimed at 210A. Resultantly, the harmonic distortion of output voltage and current meets IEEE standards according to the THD analysis shown in Fig. 4c and Fig. 4d.

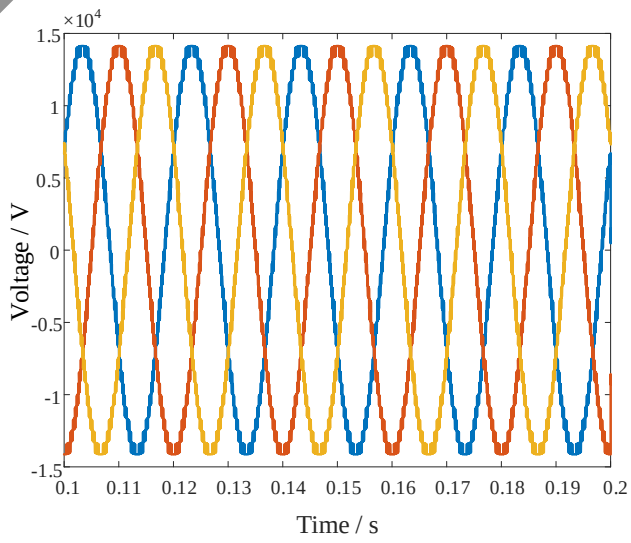

(a)

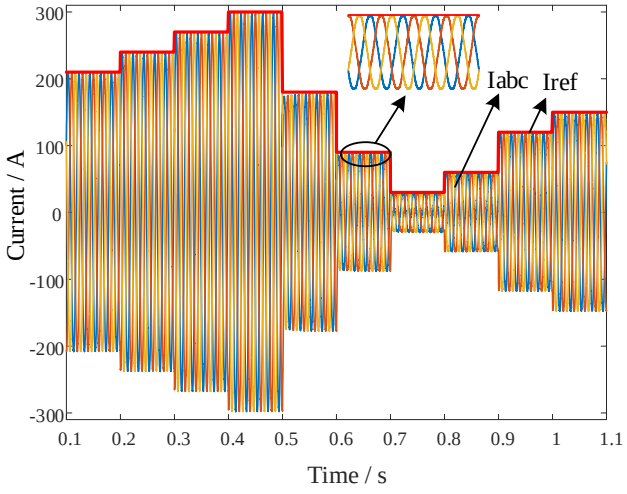

(b)

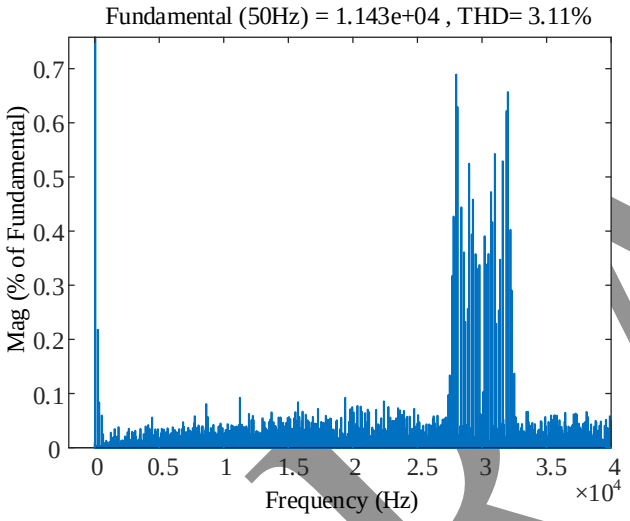

(c)

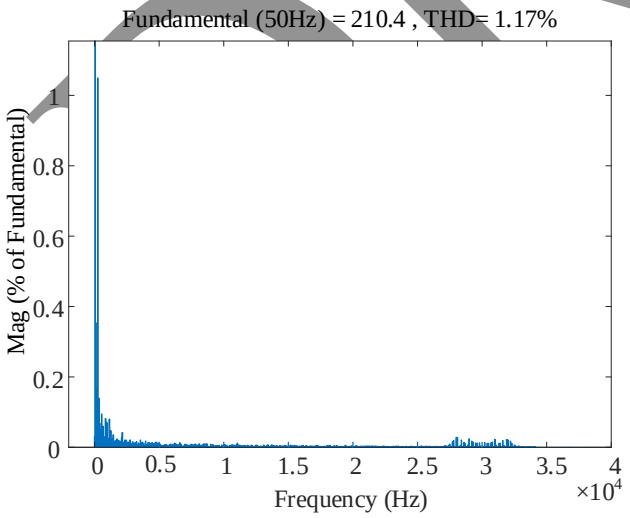

(d)

Fig. 4: Output voltage and current: (**a**) 35-level voltage (17 SMs per arm); (**b**) Three phase AC currents; (**c**) Output voltage THD; (**d**) Output current (210A) THD.

The SiC semiconductor reference is BSM300D12P3E005, and the Si device reference is FF300R12KE3; these are employed for the calculation of power losses. The calculated total power losses of the SiC-based and Si-based MMC are shown in Table 3 with reduced power losses in kilowatt and percentage. From Table 3, it is clear that the total power losses of the MMC based on the SiC switches are significantly lower than the total power losses of the MMC based on the Si switches. And Fig. 5 gives a further illustration of the relationship between the total power losses reduction and current of the SiC and Si MMC. With the increasing current, the SiC MMC yields larger total power losses compared to the Si MMC. Although the overall trend of the power losses reduction shows smaller ratio with larger current, the overall ratio of reduced losses is not less than 60%.

TABLE 2: TOTAL POWER LOSSES OF THE SIC MMC (COMPARED WITH THE SI MMC) AND LOSSES REDUCTION (SI_PLOSS-SIC_PLOSS)×100%/ SI_PLOSS

Current / A	Total losses of the SiC MMC / kW	Total losses of the Si MMC / kW	Losses reduction /kW	Losses reduction / %
30	2,89	9,35	6,46	69,1
60	3,47	12,10	8,63	71,3
90	4,27	14,98	10,71	71,5
120	5,26	17,98	12,72	70,7
150	6,45	21,02	14,57	69,3
180	7,79	24,10	16,31	67,7
210	9,26	27,23	17,97	66,0
240	10,82	30,32	19,50	64,3
270	12,45	33,49	21,04	62,8
300	14,18	36,70	22,52	61,4

*Notes: SI_PLOSS donates the total power losses of the Si MMC, and SIC_PLOSS donates the total power losses of the SiC MMC.

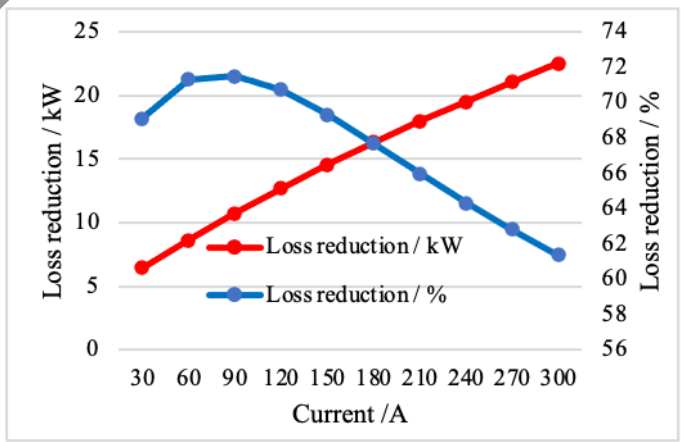

Fig. 5: Total power losses reduction versus current

VI. CONCLUSION

This paper has investigated an advancement of the MMC with the SiC switches that have lower losses in the DC microgrid applications. The MMC configuration,

mathematical modelling and control are expressed together in the power losses modeling. When the variable power input based current and voltage control performances are evaluated, the low harmonic distortion impacton the grid is achieved according to IEEE standards. Finally, the obtained results have demonstrated that the SiC devices introduced in the MMC have enhanced the performance (with more than 60% reduction of power losses) compared with conventional Si-based switches in the high-power applications, resulting in higher power efficiency for the DC microgrid systems.

ACKNOWLEDGMENT

This research study was sponsored by China Scholarship Council (CSC grant). The authors also acknowledge Flanders Make for the support to our research group.

REFERENCES

[1] A. Lesnicar and R. Marquardt, "An innovative modular multilevel converter topology suitable for a wide power range," in *2003 IEEE Bologna Power Tech Conference Proceedings*, 2003, vol. 3, pp. 272–277, doi: 10.1109/PTC.2003.1304403.

[2] H. Alyami and Y. Mohamed, "Review and development of MMC employed in VSC-HVDC systems," in *2017 IEEE 30th Canadian Conference on Electrical and Computer Engineering (CCECE)*, Apr. 2017, pp. 1–6, doi: 10.1109/CCECE.2017.7946676.

[3] Y. Zhang, X. Chen, and J. Sun, "Sequence Impedance Modeling and Analysis of MMC in Single-Star Configuration," *IEEE Trans. Power Electron.*, vol. 35, no. 1, pp. 334–346, Jan. 2020, doi: 10.1109/TPEL.2019.2911998.

[4] M. Mao *et al.*, "Multi-Objective Power Management for EV Fleet With MMC-Based Integration Into Smart Grid," in *IEEE Transactions on Smart Grid*, Mar. 2019, vol. 10, no. 2, pp. 1428–1439, doi: 10.1109/TSG.2017.2766363.

[5] M. Diaz *et al.*, "Control of modular multilevel cascade converters for offshore wind energy generation and transmission," in *2018 13th International Conference on Ecological Vehicles and Renewable Energies, EVER 2018*, 2018, pp. 1–10, doi: 10.1109/EVER.2018.8362406.

[6] A. Rashwan, "A New Topology for the Large-Scale Photovoltaic Systems Grid Connection Based on Modular Multilevel Converter," in *2018 20th International Middle East Power Systems Conference, MEPCON 2018 - Proceedings*, 2019, pp. 286–291, doi: 10.1109/MEPCON.2018.8635111.

[7] T. Soong and P. W. Lehn, "Evaluation of Emerging Modular Multilevel Converters for BESS Applications," *IEEE Trans. Power Deliv.*, vol. 29, no. 5, pp. 2086–2094, Oct. 2014, doi: 10.1109/TPWRD.2014.2341181.

[8] L. E. Zubieta and P. W. Lehn, "A high efficiency unidirectional DC/DC converter for integrating distributed resources into DC microgrids," in *2015 IEEE 1st International Conference on Direct Current Microgrids, ICDCM 2015*, 2015, pp. 280–284, doi: 10.1109/ICDCM.2015.7152054.

[9] Z. Wang, H. Lin, Y. Ma, and T. Wang, "A prototype of modular multilevel converter with integrated battery energy storage," in *2017 IEEE Applied Power Electronics Conference and Exposition (APEC)*, 2017, pp. 434–439, doi: 10.1109/APEC.2017.7930730.

[10] N. Li and F. Gao, "Linearized operation of MMC battery energy storage system," in *2016 IEEE 2nd Annual Southern Power Electronics Conference (SPEC)*, Dec. 2016, no. 1, pp. 1–5, doi: 10.1109/SPEC.2016.7846013.

[11] Z. Ma, F. Gao, X. Gu, N. Li, and D. Niu, "An Online SOH Testing Method of MMC Battery Energy Storage System," 2018, doi: 10.1109/COMPEL.2018.8460039.

[12] F. Gao, X. Gu, Z. Ma, and C. Zhang, "Redistributed Pulsewidth Modulation of MMC Battery Energy Storage System under Submodule Fault Condition," *IEEE Trans. Power Electron.*, vol. 35, no. 3, pp. 2284–2294, 2020, doi: 10.1109/TPEL.2019.2925284.

[13] Z. Ma, T. Hao, F. Gao, N. Li, and X. Gu, "Enhanced SOH balancing method of MMC battery energy storage system with cell equalization capability," in *2018 IEEE Applied Power Electronics Conference and Exposition (APEC)*, 2018, vol. 2018-March, pp. 3591–3597, doi: 10.1109/APEC.2018.8341622.

[14] K. Shenai, "Wide Bandgap (WBG) Semiconductor Power Converters for DC Microgrid Applications," in *2015 IEEE First International Conference on DC Microgrids (ICDCM)*, Jun. 2015, pp. 263–268, doi: 10.1109/ICDCM.2015.7152051.

[15] Y. Wang, A. Aksoz, T. Geury, S. B. Ozturk, O. C. Kivanc, and O. Hegazy, "A review of modular multilevel converters for stationary applications," *Appl. Sci.*, vol. 10, no. 21, pp. 1–36, 2020, doi: 10.3390/app10217719.

[16] C. Liu, D. Kong, Z. Zhang, Z. Pei, and R. Kennel, "Single-stage control system of I-MMC-Based island MVDC link receiver with multiple modulation freedoms," *IEEE Access*, vol. 8, pp. 10088–10097, 2020, doi: 10.1109/ACCESS.2020.2964839.